Competitive Heavy-Atom Tunneling Reactions Controlled Through Electronic Effects

José P. L. Roque,[1,2] Cláudio M. Nunes,[1]* Fumito Saito,[2] Bastian Bernhardt,[2] Rui Fausto,[1,3] Peter R. Schreiner[2]*

[1]University of Coimbra, CQC-IMS, Department of Chemistry, 3004-535 Coimbra, Portugal
[2]Institute of Organic Chemistry, Justus Liebig University, Heinrich-Buff-Ring 17, 35392 Giessen, Germany
[3]Faculty Sciences and Letters, Department of Physics, Istanbul Kultur University, Bakirkoy, Istanbul 34158, Turkey

ABSTRACT

Controlling QMT reactivity remains exceptionally challenging and largely unexplored, as it requires rationales distinct from those used for classical chemical reactivity. Herein, we investigated how QMT reactivity can be controlled using electronic substituent effects. Benzazirines, which have the exceptional feature to react via two competitive QMT pathways, were used as model compounds. Three novel derivatives with increasingly stronger electron-donating substituents at C4 [R = OH, $N(CH_3)_2$, and $N(CH_2)_4$] were generated in argon matrices at 3 K. Remarkably, different QMT selectivities were observed in all benzazirines. As the electron-donating strength of the substituent increases, the QMT ring-opening to nitrene starts to compete with the QMT ring-expansion to ketenimine, becoming the dominant process for the strongest electron-donating substituent [$N(CH_2)_4$]. A theoretical analysis of the substituent effects on the QMT reactivity of benzazirines was performed and compared with the experimental data for these and other C4 derivatives. Overall, the results compellingly demonstrate how subtle changes in electronic effects can be used to fine-tune QMT selectivity, and how the barrier widths, more than the barrier heights, are the determining factor.

1. INTRODUCTION

Chemical reactivity has traditionally been understood by considering that reactants transition to products by overcoming a defined transition state (TS).[1,2] This conceptual framework has guided the development of reactivity principles,[3–5] and has enabled chemists to predict and manipulate chemical reactions. However, chemical reactions driven by quantum mechanical tunneling (QMT), i.e., occurring through permeating potential energy barriers, can defy established reactivity principles, and have led to the formulation of new reactivity paradigms.[6,7] Likewise, attaining control over QMT reactions often requires alternative approaches compared to those used for non-QMT reactions, because features such as barrier widths and particle mass although essentially irrelevant in classical reactivity are pivotal in QMT reactivity. For instance, enzymologists have successfully used mutagenesis to alter the global protein dynamics and modulate hydrogen transfer distances conducive to QMT reactivity.[8] Some of us have demonstrated that specific conformational changes induced by external near-IR light on small organic molecules can activate hydrogen QMT.[9] Others have discussed the control of QMT through the application of external electric fields,[10] distinct solvation effects,[11] or isotopic labeling of key atoms.[12] Electronic substituent effects, although commonly used to modulate classical reactivity through changes in the reaction barrier height,[13,14] should have a distinct and more profound consequence on QMT reactivity through their effect on both barrier height and width.[15,16] A systematic investigation on the QMT *anti* to *syn* OD-rotamerization in *para*-substituted benzoic acids revealed that classical Hammett substituent constants σ do not correlate well with QMT rate constants and had to be replaced with QMT-specific σ^t-values.[17] In pursuit of advances to attain control over QMT reactivity, we investigate here how electronic substituent effects direct the selective outcome of competitive heavy-atom QMT reactions occurring from a single reactant.

The probability of QMT decreases exponentially with the square root of the mass of the tunneling particle. Consequently, hydrogen QMT is the predominant phenomenon in QMT chemical reactivity.[18,19] Nonetheless, experimental observation of heavy-atom QMT, involving second-row elements, was documented already in the mid-1970s,[20] and has significantly advanced in the last two decades.[21–23] Particularly noteworthy are investigations involving 2*H*-benzazirines **3**, which have provided valuable insights into heavy-atom QMT reactivity.[24–28] Derivatives of **3** can be generated by the photoisomerization of arylnitrenes **2**, which are typically accessed through denitrogenation of the corresponding arylazides **1**. However, detection of benzazirines **3** poses

significant challenges due to their highly reactive nature and QMT instability (i.e., the notion that QMT can preclude a molecule to be isolable and detected, even though it should be according to a semiclassical interpretation).[29,30] For instance, in the photochemistry of parent phenylnitrene **2a** isolated under cryogenic matrices (T = 12 K), cyclic ketenimine **4a** formed without the detection of intermediate benzazirine **3a** (Scheme 1a).[31,32] The ring-expansion of **3a** to **4a** has a computed energy barrier of a few kcal mol^{-1},[33] which should allow its capture at cryogenic temperatures. However, as shown in section 3 of the supporting information (SI), computations indicate that a very fast QMT from **3a** to **4a** should make **3a** elusive. Computations also indicate that the inclusion of electron-donating substituents at position C4 can significantly increase the ring-expansion barrier height,[34] which should decrease the QMT probability and allow the capture of benzazirine derivatives **3**. Indeed, the spectroscopic observation of heavy-atom QMT reactivity was first reported for the ring-expansion of 4-thiomethyl-2*H*-benzazirine **3b** to the corresponding ketenimine **4b** (Scheme 1b).[24] Surprisingly, some of us later revealed that in the case of 4-amino-2*H*-benzazirine **3c**, the potential energy surface (PES) is sufficiently affected to allow for the QMT ring-opening to **2c**, which can efficiently compete with the QMT ring-expansion to **4c**, with a product distribution **2c:4c** of 15:85 (Scheme 1c).[27]

The discovery of two competitive QMT pathways in benzazirines **3** establishes these species as ideal systems for investigating electronic substituent effects in the selectivity of QMT reactions. In this context, we considered the inclusion of increasingly stronger electron-donating substituents at position C4, selecting them based on the values of Hammett substituent constants (σ) (Scheme 2).[35] Thus, first the hydroxyl substituent [σ_p(OH) = −0.37] was chosen to bridge the electron-donating strengths of the previously studied thiomethyl [$\sigma_p(SCH_3)$ = 0.00] and amino [$\sigma_p(NH_2)$ = −0.66] substituents. Then, the dimethylamine substituent [$\sigma_p(N(CH_3)_2)$ = −0.83] was selected to provide an electron-donating strength superior to that of the amino substituent. Finally, the 1-pyrrolidine ($N(CH_2)_4$) substituent was chosen as potentially the strongest electron-donating substituent (even though its Hammett constant is unknown). Herein, we report the successful generation of the three novel C4-substituted benzazirine targets (**3d**, **3e**, and **3f**) in argon matrices at 3−18 K. We investigated their QMT reactivities and analyzed the effects of C4 substitution on the competitive QMT ring-opening *vs.* QMT ring-expansion reactions. Our findings emphasize the profound influence of substitution on QMT reactivity and selectivity, surpassing the conventional expectation solely based on reaction barrier height, which typically governs classical reactivity.

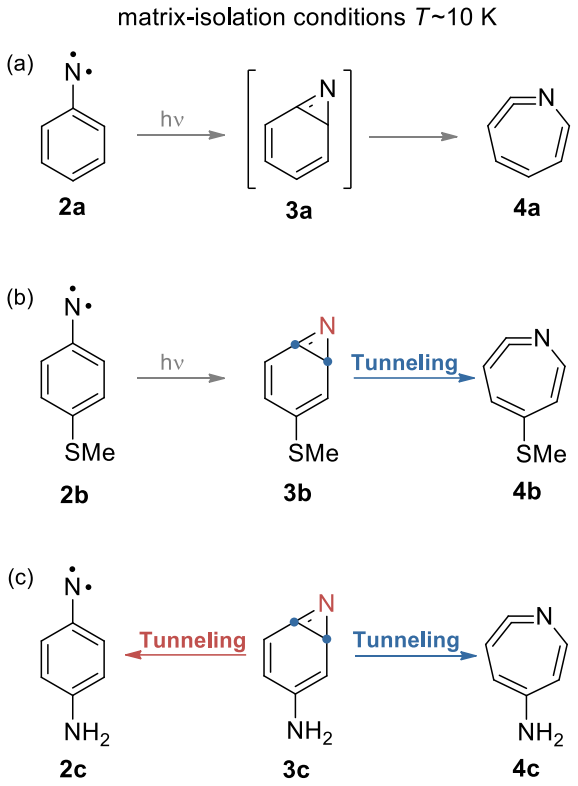

Scheme 1. Summary of results reported under matrix-isolation conditions: (a) The photochemistry of phenylnitrene **2a** yields only ketenimine **4a**;[31] (b) the photochemistry of nitrene **3b** yields 4-thiomethyl-2*H*-benzazirine **3b** which then undergoes QMT ring-expansion to ketenimine **4b**;[24] (c) 4-amino-2*H*-benzazirine **3c** undergoes competitive QMT ring-opening to **2c** vs QMT ring-expansion to **4c** (**2c:4c** = 15:85).[27]

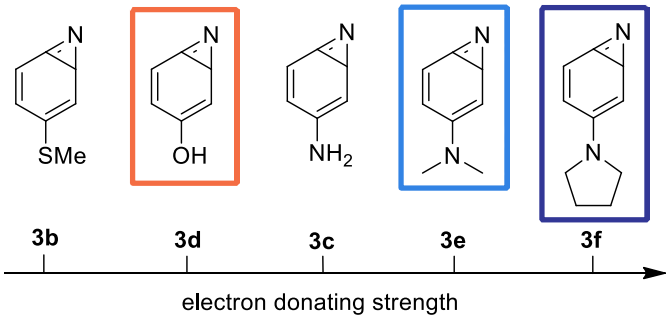

Scheme 2. 2*H*-Benzazirines with progressively stronger electron-donating substituents at position C4. The generation and QMT reactivity of benzazirines **3d**, **3e**, and **3f** are described for the first time in this study, whereas those of **3b** and **3c** were previously reported.[24,27]

2. RESULTS AND DISCUSSION

2.1. Direct Observation of QMT Reactivity in 4-Substituted-2*H*-Benzazirines

2.1.1. 4-Hydroxy-2*H*-Benzazirine

The 4-hydroxy-phenylazide **1d** precursor was synthesized and monomers of the sample were isolated in an Ar matrix at 3.5 K (details are given in Sections 1.1 and 1.2 of the SI). The corresponding IR spectrum shows the most characteristic ν(OH) and $\nu(N_3)_{as}$ bands at 3645/3634 and 2119/2078 cm^{-1} (Figure S2 and Table S1).[36] The subsequent photolysis of **1d** was induced at 260 nm, and it generated triplet 4-hydroxy-phenylnitrene ^{3}**2d** (minor amount) and 5-hydroxy-1-aza-1,2,4,6-cycloheptatetraene **4d** (major amount) (Figure S3). Supported by previous UV-Vis spectroscopic data and photochemistry experiments on similar species,[27] we found that subsequent irradiation at 350 nm completely converted ketenimine **4d** to triplet nitrene ^{3}**2d** (Figure S4). Characteristic IR bands of ^{3}**2d** were identified at 1573, 1278, 1170, and 816 cm^{-1} in agreement with the B3LYP/6-311+G(2d,p) computed vibrational modes of ^{3}**2d** at 1576 [ν(CC)], 1267 [ν(CO)], 1155 [δ(OH)], and 813 [γ(CH)] cm^{-1}. Distinctive IR bands of **4d** were observed at 1891, 1591, 1305, 1147, and 796 cm^{-1} in agreement with the computed vibrational modes of **4d** at 1903 $[\nu(C{=}C{=}N)_{as}]$, 1593 $[\nu(C{=}C)_{as}]$, 1309 $[\nu(C{=}C{=}N)_{s}]$, 1148 [ν(CO) − δ(OH)], and 799 [γ(CH)] cm^{-1}. A more detailed assignment of the IR spectra of ^{3}**2d** and **4d** is provided in Tables S2 and S3. The Ar matrix enriched with ^{3}**2d** was then irradiated at 435 nm, which allowed the generation of target 4-hydroxy-2*H*-benzazirine **3d** efficiently (Figure S5). Characteristic IR bands of **3d** were observed at 1716, 1594, 1235, 1172/1149, and 808 cm^{-1} in good correspondence with the computed vibrational transitions of **3d** at 1749 [ν(C=N)], 1593 $[\nu(C{=}C)_{as}]$, 1228 [ν(CO) + δ(OH)], 1155 [ν(CO) − δ(OH)], and 811 [γ(CH)] cm^{-1}. Comprehensive assignments of the IR spectra of **3d** are presented in Table S4.

4-Hydroxy-2*H*-benzazirine **3d** spontaneously undergoes ring-expansion reaction to ketenimine **4d** in the dark (Figure 1 and Scheme 3). The putative formation of triplet nitrene ^{3}**2d** was excluded based on the absence of its signals in the corresponding difference IR spectrum. The kinetics of the spontaneous reaction of ^{3}**2d** to **4d** was measured in an Ar matrix at 3.5 and 18 K by collecting IR spectra over time using a longpass filter blocking light above 2200 cm^{-1} (details given in the section 1.5 of the SI). Approximate rate constants of $k_{\mathbf{3d}(3.5K)} = 3.4 \times 10^{-5}$ s^{-1} ($\tau_{1/2}$ = 5.6 h) and $k_{\mathbf{3d}(18K)} = 3.9 \times 10^{-5}$ s^{-1} ($\tau_{1/2}$ = 4.9 h) were obtained by fitting the experimental data with

first-order exponential decay equations (Figure S6). The essentially unchanged reaction rates upon an up to five-fold increase of the temperature provides strong evidence for the occurrence of QMT in the ring-expansion of **3d** to **4d**. The contribution of IR-induced reactivity resulting from the short-time exposure to filtered IR light ($\tilde{\nu}$ > 2200 cm^{-1}) during spectral acquisition was found to be negligible (details are given in the section 1.5 of the SI).

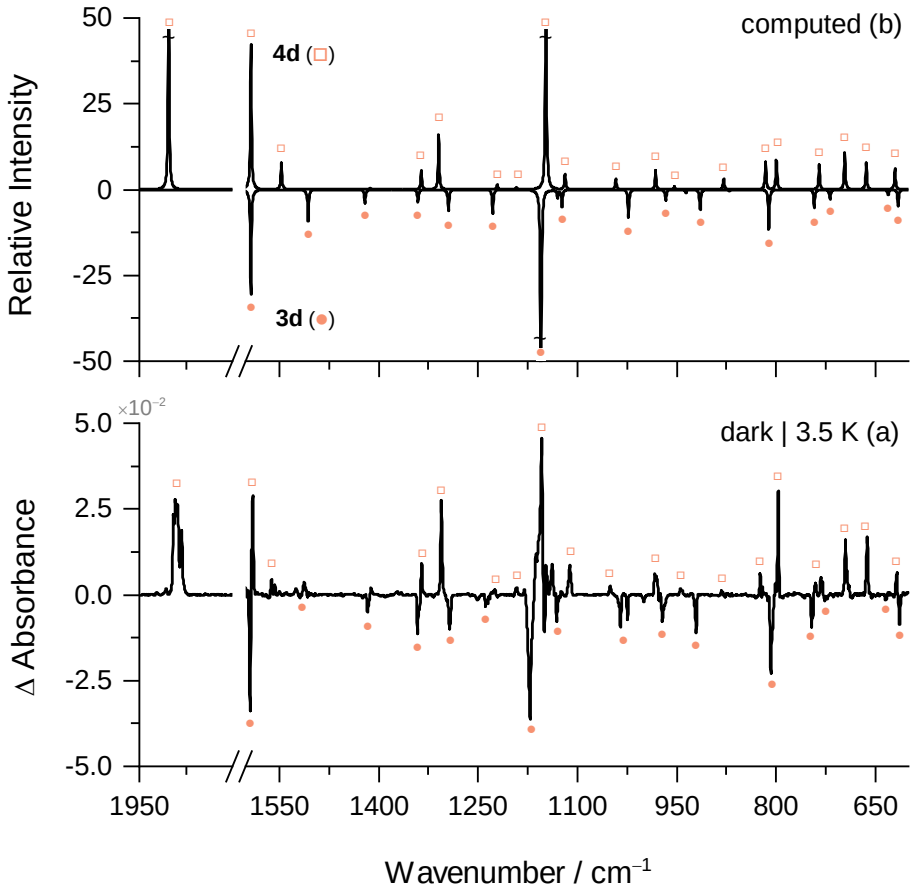

Figure 1. (a) Experimental difference IR spectrum showing changes after keeping 4-hydroxy-2*H*-benzazirine **3d** in an Ar matrix at 3.5 K in the dark for 8 h. The downward IR bands are due to the consumption of **3d** and the upward IR bands due to the formation of 5-hydroxy-1-aza-1,2,4,6-cycloheptatetraene **4d**. (b) Computed B3LYP/6-311+G(2d,p) IR spectra of **3d** (negative bands, orange circles) and **4d** (positive bands, orange squares).

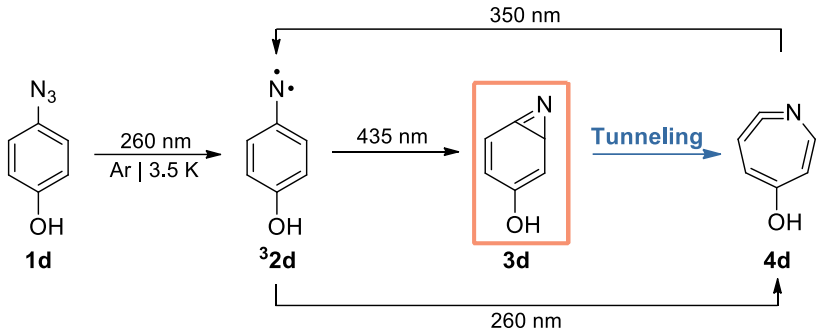

Scheme 3. Summary of the observed reactivity involving 4-hydroxy-2*H*-benzazirine **3d** generated in an Ar matrix at 3.5 K.

2.1.2. 4-Dimethylamino-2*H*-Benzazirine

Monomers of the 4-dimethylamino-phenylazide **1e** precursor were isolated in an Ar matrix at 3.5 K (details given in sections 1.1 and 1.2 of the SI). The corresponding IR spectrum and vibrational assignments are provided in Figure S8 and Table S5. The subsequent photolysis of **1e** induced at 255 nm gives triplet 4-dimethylamino-phenylnitrene ^{3}**2e** as the exclusive product (Figure S9). Characteristic IR bands of ^{3}**2e** were observed at 1588, 1369, 1325, 944, and 803 cm^{-1} in a good match with the B3LYP/6-311+G(2d,p) computed vibrations of ^{3}**2e** at 1588 [ν(CC)], 1356 [$\nu(CN_{dme})$], 1313 [$\nu(CN_{nit})$], 933 [$\nu(N(CH_3)_2)_s$], and 800 [$\gamma(CH)_{ring}$] cm^{-1}. A comprehensive assignment of the IR spectrum of ^{3}**2e** is given in Table S6. The matrix enriched with triplet nitrene ^{3}**2e** was then irradiated at 450 nm yielding a mixture of 4-dimethylamino-2*H*-benzazirine **3e** and 5-dimethylamino-1-aza-1,2,4,6-cycloheptatetraene **4e** (Figure S10).

Benzazirine **3e** spontaneously rearranges in the dark to give both triplet nitrene ^{3}**2e** and ketenimine **4e** (Figure 2 and Scheme 4). Distinctive IR bands of **3e** appear at 1728, 1494, 1317, 934, and 794/785 cm^{-1} in agreement with the computed vibrational modes of **3e** at 1754 [ν(C=N)], 1495 [$\nu(C=C)_s$], 1313 [$\nu(CN_{dme})$], 922 [$\nu(N(CH_3)_2)_s$], and 811 [$\gamma(CH)_{ring}$] cm^{-1}. A detailed assignment of the IR spectrum of **3e** is provided in Table S7. After the complete transformation of **3e**, irradiation at 350 nm induces the clean conversion of **4e** to ^{3}**2e** (Figure S11). Characteristic IR bands of ketenimine **4e** appear at 1886, 1580, 1333, 1125, and 678 cm^{-1} in good correspondence with the computed IR spectral bands of **4e** at 1901 [$\nu(C=C=N)_{as}$], 1579 [$\nu(C=C)_{as}$], 1327 [$\nu(CN_{dme})$], 1121 [$\nu(C=C=N)_s$], and 681 [$\gamma(CH)_{ring}$] cm^{-1}. A more extensive assignment of the IR spectrum of **4e** is given in Table S8. Based on the IR spectral information regarding the

photoreaction of **4e** to ^{3}**2e**, the spontaneous rearrangement of **3e** in the dark could be estimated to produce a ^{3}**2e**:**4e** ratio of 30:70 (details are given in the section 1.4 of the SI).

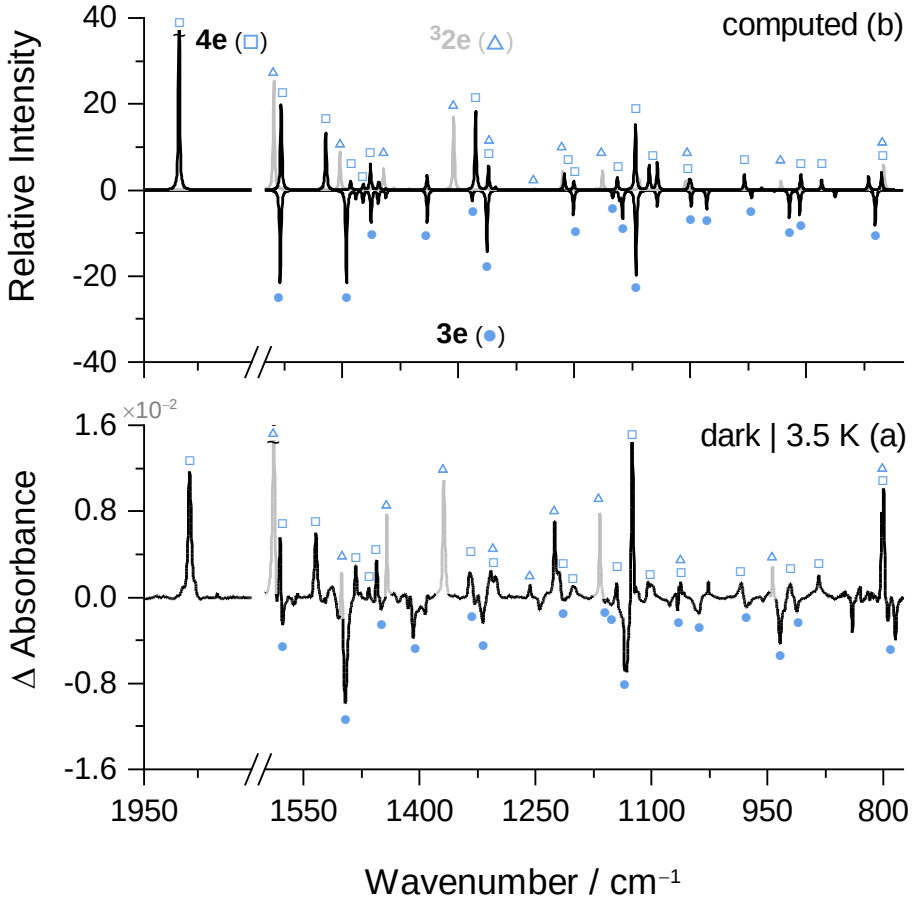

Figure 2. (a) Experimental difference IR spectrum showing changes after keeping 4-dimethylamino-2*H*-benzazirine **3e** in an Ar matrix at 3.5 K in the dark for 24 h. The downward bands are due to the consumption of **3e** and the upward bands due to the formation of triplet 4-dimethylamino-phenylnitrene ^{3}**2e** and 5-dimethylamino-1-aza-1,2,4,6-cycloheptatetraene **4e**. (b) Computed B3LYP/6-311+G(2d,p) IR spectrum of **3e** (black line, blue circles), ^{3}**2e** (gray line, blue triangles), and **4e** (black line, blue squares). The intensities of the computed IR bands **3e**, ^{3}**2e**, and **4e** were multiplied by −1.0, 0.3, and 0.7, respectively.

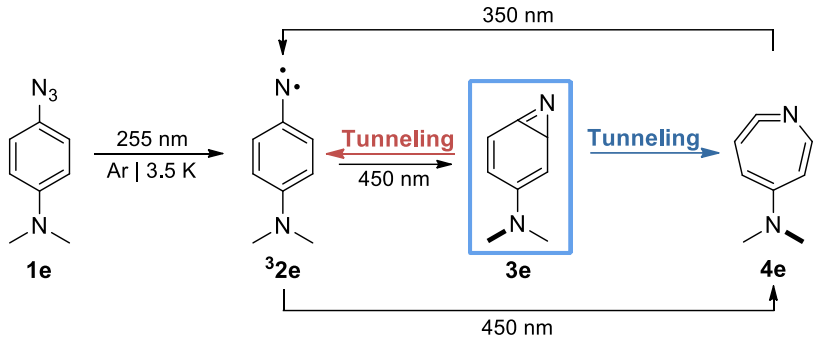

Scheme 4. Summary of the observed reactivity involving 4-dimethylamino-2*H*-benzazirine **3e** generated in an Ar matrix at 3.5 K.

The kinetics of the spontaneous transformation of **3e** was measured in Ar matrices at 3.5 and 18 K by collecting several IR spectra over time using a longpass filter blocking light above 2200 cm^{-1} (otherwise the sample was kept in the dark). Approximate rate constants of $k_{\mathbf{3e}(3.5K)}$ = 3.7×10^{-5} s^{-1} ($\tau_{1/2}$ = 5.2 h) and $k_{\mathbf{3e}(18K)}$ = 3.9×10^{-5} s^{-1} ($\tau_{1/2}$ = 5.0 h) were obtained by fitting the experimental data with first-order exponential decay equations (Figure S12). The observation of similar reaction rates at temperatures of 3.5 and 18 K strongly indicates the occurrence of QMT. Moreover, the ^{3}**2e**:**4e** product ratio from the spontaneous transformation of **3e** was estimated to be identical at 3.5 and 18 K (30:70 *vs* 33:67, respectively). These data clearly support the occurrence of two independent and competitive QMT reactions, namely the QMT ring-opening of **3e** to ^{3}**2e** and the QMT ring-expansion of **3e** to **4e**. Considering a first-order reaction of a single reactant to give two different products, approximate rate constants of $k_{\mathbf{2e}(3.5K)}$ = 1.1×10^{-5} s^{-1} ($\tau_{1/2}$ = 17.3 h) and $k_{\mathbf{4e}(3.5K)}$ = 2.6×10^{-5} s^{-1} ($\tau_{1/2}$ = 7.4 h) were obtained for the QMT formation of ^{3}**2e** and **4e**, respectively. The contribution of IR-induced reactivity resulting from the short-time exposure to filtered IR light ($\tilde{\nu}$ > 2200 cm^{-1}) during spectral acquisition was found to be negligible (details are given in the section 1.5 of the SI).

2.1.3. 4-Pyrrolidine-2*H*-Benzazirine

The 4-pyrrolidine-phenylazide **1f** precursor was prepared and monomers were deposited in an Ar matrix at 3.5 K (Figure S14 and Table S9; details are given in sections 1.1 and 1.2 of the SI). The photolysis of **1f** at 255 nm produces triplet 4-pyrrolidine-phenylnitrene ^{3}**2f** as the sole product (Figure S15). Distinctive IR bands of ^{3}**2f** were observed at ~1589, ~1464, 1384, 1322, and 802

cm^{-1} in good correspondence with the B3LYP/6-311+G(2d,p) computed vibrational modes of ^{3}**2f** at 1590 [ν(CC)], 1463 [$\nu(CN_{pyr})$ + ν(CC)], 1379 [$\nu(CN_{pyr})$ − ν(CC)], 1314 [$\nu(CN_{nit})$], and 799 [$\gamma(CH)_{ring}$] cm^{-1}. A more complete assignment of the IR spectrum of ^{3}**2f** is presented in Table S10. The generation of the target 4-pyrrolidine-2*H*-benzazirine **3f** was challenging and only a small amount could be isolated after short-time irradiation (a few minutes) of ^{3}**2f** at 450 nm (Figure S16). The 5-pyrrolidine-1-aza-1,2,4,6-cycloheptatetraene **4f** formed as the major product. Clean re-conversion of ketenimine **4f** to triplet nitrene ^{3}**2f** was achieved by irradiation of **4f** at 350 nm (Figure S17). Characteristic IR bands of **4f** appear at ~1873, 1584, 1337, 1113, and 779 cm^{-1} in good match with the computed vibration of **4f** at 1884 [$\nu(C{=}N{=}C)_{as}$], 1583 [$\nu(C{=}C)_{as}$], 1334 [$\nu(CN_{pyr})$], 1116 [$\nu(C{=}C{=}N)_{s}$ + δ(CH)], and 787 [$\gamma(CH)_{ring}$] cm^{-1}. Comprehensive assignments of the IR spectrum of **4f** are given in Table S11.

Benzazirine **3f** spontaneously rearranges in the dark to give both triplet nitrene ^{3}**2f** and ketenimine **4f** (Figure 3 and Scheme 5). Distinctive IR bands of **3f** were observed at 1718, 1579, 1482, 1341/1335, ~943, and 773 cm^{-1} in agreement with the computed vibrational transitions of **3f** at 1745 [ν(C=N)], 1582 [$\nu(C{=}C)_{as}$], 1477 [$\nu(C{=}C)_{s}$], 1331/1323 [$\nu(CN_{pyr})$ +/− δ(CH)], 930 [$\nu(N(CH_2)_2)_{s}$], and 784 [$\gamma(CH)_{ring}$] cm^{-1}. A more detailed assignment of the IR spectrum of **3f** is presented in Table S12. The kinetics of the spontaneous rearrangement of **3f** was measured in Ar matrices at 3.5 and 18 K, and approximate rate constants of $k_{\mathbf{3f}(3.5K)} = 3.4 \times 10^{-4}$ s^{-1} ($\tau_{1/2}$ = 34 min) and $k_{\mathbf{3f}(18K)} = 4.4 \times 10^{-4}$ s^{-1} ($\tau_{1/2}$ = 26 min) were obtained (Figure S18). A ^{3}**2f**:**4f** product ratio of 71:29 and 75:25 was measured at 3.5 and 18 K, respectively. The observation of similar reaction rates after increasing the temperature by a factor of five, associated with the formation of an equivalent product ratio, clearly indicates the occurrence of competitive QMT ring-opening of **3f** to ^{3}**2f** and QMT ring-expansion of **3f** to **4f**. Approximate rate constants of $k_{\mathbf{2f}(3.5K)} = 2.4 \times 10^{-4}$ s^{-1} ($\tau_{1/2}$ = 48 min) and $k_{\mathbf{4f}(3.5K)} = 9.9 \times 10^{-5}$ s^{-1} ($\tau_{1/2}$ = 117 min) were estimated for the QMT formation of ^{3}**2f** and **4f**, respectively (details are given in the section 1.5 of the SI). The contribution of IR-induced reactivity resulting from the short-time exposure to filtered IR light ($\tilde{\nu} > 2200$ cm^{-1}) during spectral acquisition was found to be negligible (details are given in the section 1.5 of the SI).

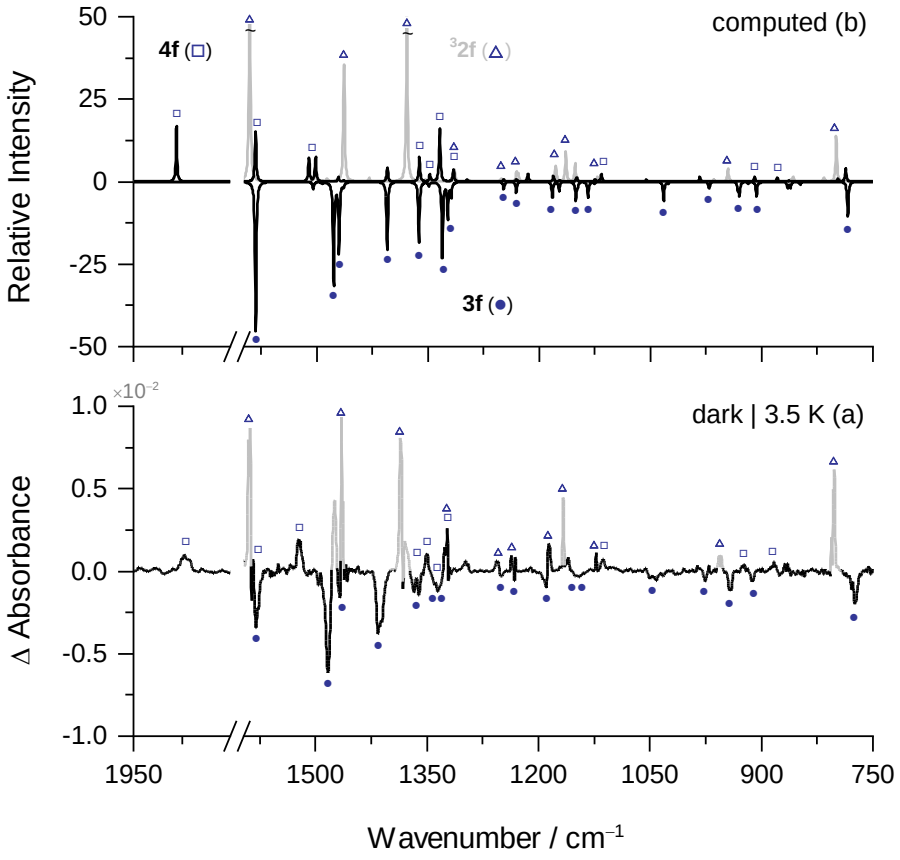

Figure 3. (a) Experimental difference IR spectrum showing changes after keeping 4-pyrrolidine-2*H*-benzazirine **3f** in an Ar matrix at 3.5 K in the dark for 1 h. The downward bands are due to the consumption of **3f** and the upward bands due to the formation of triplet 4-pyrrolidine-phenylnitrene ^{3}**2f** and 5-pyrrolidine-1-aza-1,2,4,6-cycloheptatetraene **4f**. (b) Computed B3LYP/6-311+G(2d,p) IR spectrum of **3f** (black line, dark blue circles), ^{3}**2f** (gray line, dark blue triangles), and **4f** (black line, dark blue squares). The intensities of the computed IR bands **3f**, ^{3}**2f**, and **4f** were multiplied by −1.0, 0.7, and 0.3, respectively.

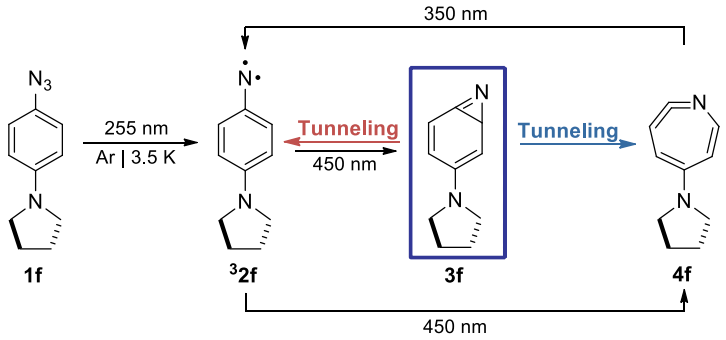

Scheme 5. Summary of the observed reactivity involving 4-pyrrolidine-2*H*-benzazirine **3f** generated in an Ar matrix at 3.5 K.

2.2. Computations of QMT Reactivity in 4-Substituted-2*H*-Benzazirines

To deepen our knowledge about the substituent effects on the possible competitive QMT reactions of benzazirines **3**, we computed the corresponding potential energy surfaces (PES) and QMT rates. The NEVPT2(8,8)/6-311+G(2d,p)//CASSCF(8,8)/6-311+G(2d,p) method was employed to compute the ring-opening reaction of **3d-f** to ^{1}**2d-f** (the subsequent ISC to ground-state ^{3}**2d-f** should occur much faster and not affect the reaction rates). This method was chosen because a multireference method with dynamic correlation is needed to correctly describe open-shell singlet nitrenes ^{1}**2d-f** and the corresponding reaction path from **3d-f**. The CCSD(T)/cc-pVTZ//B3LYP/6-311+G(2d,p) method was employed to compute the ring-expansion reaction of **3d-f** to **4d-f**. This method provides accurate energies for the single-reference wavefunction species involved in this reaction. Vibrationally adiabatic surfaces were computed using intrinsic reaction coordinates (IRC) with vibrational energy corrections containing all modes orthogonal to the reaction path. The QMT rates were then calculated by numerically integrating the corresponding permeation barrier using the Wentzel-Kramers-Brillouin (WKB) equations as implemented in TUNNEX.[37] The overall approach is equivalent to the one previously used to compute the competitive QMT reactions of **3c**,[27] which demonstrates reasonably good agreement with experimental results (details are given in sections 2.2 and 2.3 of SI).

For 4-hydroxy-2*H*-benzazirine **3d**, computations estimate a barrier height for the ring-opening to ^{1}**2d** of 3.8 kcal mol^{-1} and for the ring-expansion to **4d** of 7.7 kcal mol^{-1} (Figure S20). In contrast to the reaction barrier height, the barrier width is substantially larger for **3d** → ^{1}**2d** than for **3d** → **4d**, 7.58 *vs.* 4.11 amu$^{1/2}$ bohr, respectively (Figure 4).[38] Although irrelevant from the classical point of view of chemical reactivity, the barrier width is a crucial factor to determine QMT reactivity and the emergence of tunneling control.[7] Interestingly, this scenario is clearly manifested in the reactivity of **3d**, with computations estimating QMT rate constants of 2.8×10^{-11} s^{-1} for the ring-opening **3d** → ^{1}**2d** ($\tau_{1/2}$ ~790 a) and of 2.0×10^{-4} s^{-1} for the ring-expansion **3d** → **4d** ($\tau_{1/2}$ ~1 h). These theoretical results show good agreement with the experimental observation of tunneling control and exclusive QMT ring-expansion of **3d** to **4d** ($\tau_{1/2}$ ~5 h).

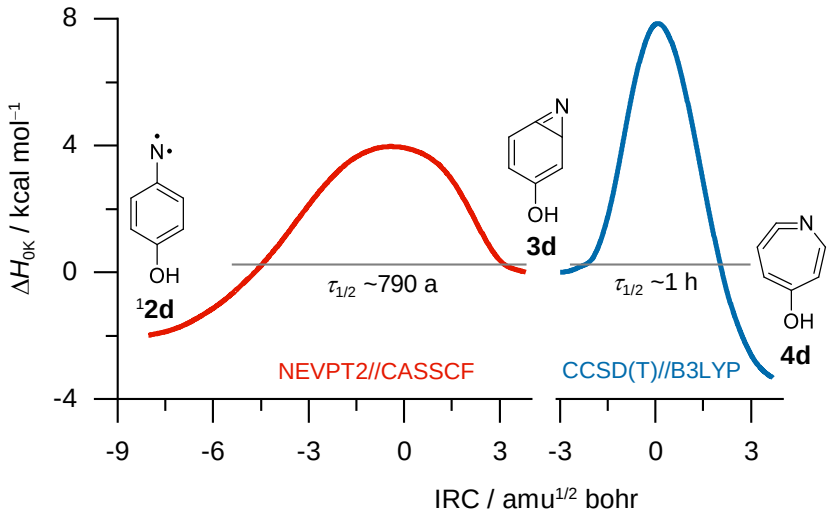

Figure 4. The intrinsic reaction coordinate (IRC) profiles for **3d** → **^{1}2d** and **3d** → **4d** reactions computed at the NEVPT2(8,8)/6-311+G(2d,p)//CASSCF(8,8)/6-311+G(2d,p) and CCSD(T)/cc-pVTZ//B3LYP/6-311+G(2d,p) levels of theory, respectively. The IRC energies are relative to the absolute energy of **3d** and include ZPVE corrections of $3N-7$ vibrations. The gray horizontal line represents half of the collision frequency. The QMT half-lives $\tau_{1/2}$ from the vibrational ground state of **3d** were computed using the WKB approach (section 2.3 of the SI).

For 4-dimethylamino-2*H*-benzazirine **3e**, the computations turn out to be troublesome and did not provide sufficiently accurate PESs to enable reliable calculations of QMT reaction rates. The PESs associated with reactions **3e** → **^{1}2e** and **3e** → **4e** must account for the rotation of the dimethylamine group because it adopts different orientations in **^{1}2e**, **3e**, and **4e** (a detailed discussion is given in section 4 of the SI). The computations at CASSCF/6-311+G(2d,p) and NEVPT2(8,8)/6-311+G(2d,p)//CASSCF(8,8)/6-311+G(2d,p) levels estimate similar barrier heights of ~3.1 kcal mol^{-1} for the ring-opening **3e** → **^{1}2e**. However, the CASSCF method fails to describe the correct geometry of **^{1}2e** and finds a global minimum in which the dimethylamine group adopts a significative out-of-plane geometry. NEVPT2 single-point corrections show that such a geometry is energetically higher by 1.7 kcal mol^{-1} than a nearly-planar one. Because of the incompatibility of the methods, implementing NEVPT2 single point corrections on top of the IRC computed at the CASSCF level would not improve the accuracy of the PES (Figure S22). In fact, the computed QMT rate using the CASSCF PES (k = 4.0 × 10^{-6} s^{-1}; $\tau_{1/2}$ = 48 h) is in better agreement with experimental measurements ($k_{\mathbf{2e}(3.5\text{K})}$ = 1.1 × 10^{-5} s^{-1}; $\tau_{1/2}$ = 17.3 h) than the computed QMT rate using the NEVPT2//CASSCF PES (k = 3.6 × 10^{-10} s^{-1}; $\tau_{1/2}$ = 60 a). For **3e** →

4e, two distinct transition states (TSs) were found connecting the minima. The PES associated to the lower-lying **TS'** (7.5 kcal mol^{-1} at the CCSD(T)/cc-pVTZ//B3LYP/6-311+G(2d,p) level) requires a ~60° rotation of the dimethylamine group prior to reaching the TS, which precludes the occurrence of QMT (Figure S23a). In case of the PES associated to the higher-lying **TS''** (8.7 kcal mol^{-1} at the CCSD(T)/cc-pVTZ//B3LYP/6-311+G(2d,p) level), the ~60° rotation of the dimethylamine group occurs after the TS. In the PES computed at B3LYP/6-311+G(2d,p), such rotation does not affect the permeation barrier because it occurs after the QMT process (outside the PES turning points) (Figure 23b). The corresponding computed QMT rate is $k = 8.4 \times 10^{-6}\ s^{-1}$ ($\tau_{1/2}$ = 23 h), which is in (fortuitous) agreement with the experimental measurements ($k_{\mathbf{4e}(3.5K)} = 2.6 \times 10^{-5}\ s^{-1}$; $\tau_{1/2}$ = 7.4 h). However, implementing CCSD(T) single point corrections on top of the IRC computed at the B3LYP level leads to a PES that now includes some rotation of the dimethylamine group in the QMT process (within the PES turning points) (Figure 23c). This modification significantly increases the permeation barrier and consequently leads to an extremely low QMT rate ($k = 2.6 \times 10^{-19}\ s^{-1}$; $\tau_{1/2} = 8.5 \times 10^{10}$ a). Overall, even though these computations fail to yield sufficiently accurate rate constants, they provide important insights by revealing that the shape of the PESs can enormously affect the QMT probabilities.[15]

For 4-pyrrolidine-2*H*-benzazirine **3f**, computations estimate a barrier height for the ring-opening to **^{1}2f** of 1.4 kcal mol^{-1} and for the ring-expansion to **4f** of 8.0 kcal mol^{-1} (Figure S24). A second conformer **3f'**, differing from **3f** by distinct ring-puckering of the pyrrolidine ring, was also found. The IR spectral signatures of the **3f** and **3f'** are virtually indistinguishable. However, according to the computations, conformer **3f'** is thermodynamically and kinetically less stable than **3f** (Figure S24), and it should not be isolable due to very fast QMT (**3f'** → **^{1}2f** barrier height is 0.8 kcal mol^{-1} and the corresponding QMT rate is $k = 3.0 \times 10^{7}\ s^{-1}$; $\tau_{1/2} \sim 2.3 \times 10^{-8}$ s).[39] Therefore, it is reasonable to assume that only the most stable **3f** and its corresponding QMT transformations were observed in the matrix-isolation experiments. For this scenario, computations estimate the QMT ring-opening **3f** → **^{1}2f** with $k = 1.3 \times 10^{3}\ s^{-1}$ ($\tau_{1/2}$ = 0.5 ms) to be considerably faster than the QMT ring-expansion **3f** → **4f** with $k = 1.6 \times 10^{-5}\ s^{-1}$ ($\tau_{1/2}$ = 12 h) (Figure 5). Although significantly overestimating the rate of the former reaction, computations show qualitative agreement with the experimental observation of QMT being faster for the ring-opening **3f** → **^{1}2f** ($k_{\mathbf{2f}(3.5K)} = 2.4 \times 10^{-4}\ s^{-1}$; $\tau_{1/2}$ = 48 min) than for the ring-expansion **3f** → **4f** ($k_{\mathbf{4f}(3.5K)} = 9.9 \times 10^{-5}\ s^{-1}$; $\tau_{1/2}$ = 2 h), and the contrasting QMT reactivity in comparison to **3d**.

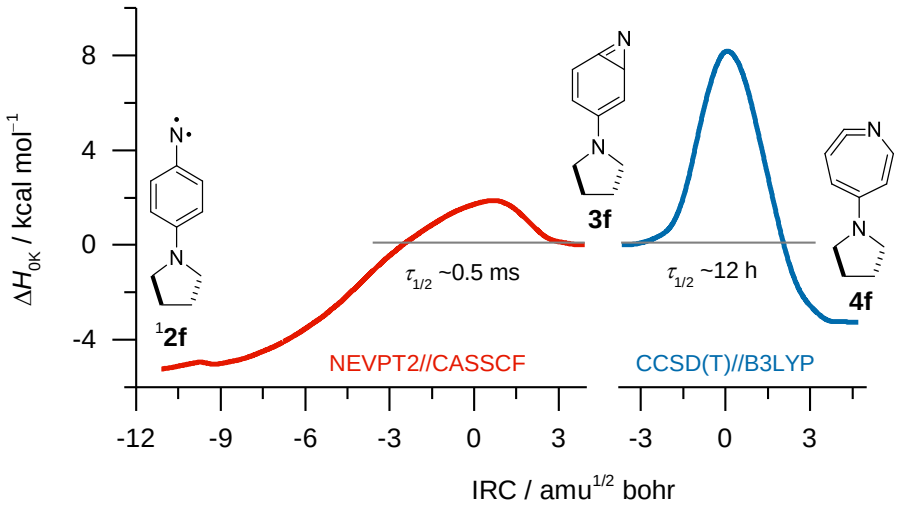

Figure 5. The intrinsic reaction coordinate (IRC) profiles for **3f** → ^{1}**2f** and **3f** → **4f** reactions computed at the NEVPT2(8,8)/6-311+G(2d,p)//CASSCF(8,8)/6-311+G(2d,p) and CCSD(T)/cc-pVTZ//B3LYP/6-311+G(2d,p) levels of theory, respectively. The IRC energies are relative to the absolute energy of **3f** and include ZPVE corrections of 3*N*−7 vibrations. The gray horizontal line represents half of the collision frequency. The QMT half-lives $\tau_{1/2}$ from the vibrational ground state of **3f** were computed using the WKB approach (section 2.3 of the SI).

2.3 Assessing the Substituent Effect on the QMT Reactivity of 2*H*-Benzazirines

To better understand how the two possible competitive QMT reactions of benzazirines **3** are differently affected by the nature of the C4 substituent, a detailed comparative analysis was conducted on the computational and experimental results obtained for the C4-substituted derivatives (Scheme 2).

Considering the unsubstituted derivative (R = H) as reference (Figure 6), the computations indicate that the **3** → ^{1}**2** ring-opening energy barrier decreases as the electron-donating strength of the C4 substituent increases [from 5.4 kcal mol^{-1} for R = H down to 1.4 kcal mol^{-1} for R = N(CH$_2$)$_4$]. Concomitantly, the corresponding reaction enthalpies significatively decreases as the electron-donating strength of the C4 substituent increases [from −0.9 kcal mol^{-1} for R = H down to −5.7 kcal mol^{-1} for R = N(CH$_2$)$_4$]. On the other hand, computations show that the **3** → **4** ring-expansion energy barrier increases for all C4 electron-donating substituents, but without correlating to their respective strength [from 5.1 kcal mol^{-1} for R = H up to 7.3−8.0 kcal mol^{-1} for R = NH$_2$, OH, and N(CH$_2$)$_4$]. The corresponding reaction enthalpies at most only slightly increase for the C4 electron-donating substituents and, again, without any correlation with their respective

donor strength [varying between −4.5 kcal mol^{-1} for R = H and NH_2 to −3.2 kcal mol^{-1} for R = OH]. The pronounced effect and correlation trend found between the electron-donating strength of the C4 substituents and the energy barriers or reaction enthalpies for the **3** → ^{1}**2** ring-opening can be partially rationalized by the stabilization of the open-shell nitrenes ^{1}**2**, which are electron-deficient species characterized by a quinoid-type structure with one unpaired electron localized mainly at the C4 carbon of the ring (Figure 6).

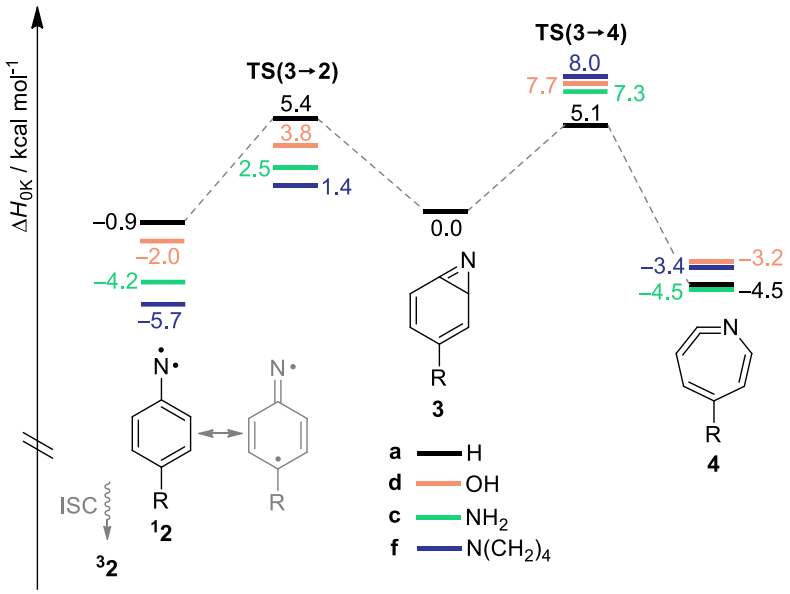

Figure 6. Energy profiles (ΔH_{0K} in kcal mol^{-1}) for **3** → ^{1}**2** ring-opening and **3** → **4** ring-expansion reactions with R = H (**3a**), OH (**3d**), NH_2 (**3c**) and $N(CH_2)_4$ (**3f**) computed at the NEVPT2(8,8)/6-311+G(2d,p)//CASSCF(8,8)/6-311+G(2d,p) and CCSD(T)/cc-pVTZ//B3LYP/6-311+G(2d,p) levels of theory, respectively. Energy values are relative to the energy of the corresponding benzazirines **3**. For the R = SCH_3 (**3b**) and R = $N(CH_3)_2$ (**3e**) derivatives, the rotamerization of this substituent occurs concomitantly with the ring-opening or ring-expansion reaction, which makes it difficult to compute the corresponding PES accurately (see, *e.g.*, section 4 of the SI).

A particularly distinguishing feature of QMT reactivity is its high dependence on the barrier width of the reaction, which differs from classical reactivity that depends only on the barrier height.[15,40] Indeed, computations show that for the unsubstituted **3a**, although the ring-opening **3a** → ^{1}**2a** and ring-expansion **3a** → **4a** reactions have approximately the same barrier heights (~5 kcal mol^{-1}), the QMT ring-opening rate is 19 orders of magnitude faster than the QMT ring-expansion rate (Table 1). The key difference is the respective barrier widths, 8.63 *vs.* 3.22

amu$^{1/2}$ bohr (Figure S1).[38] Therefore, to achieve QMT reactivity control through substituent electronic effects, it is pivotal to capture their influence on the barrier width (more so than their influence on the barrier height), which might be roughly rationalized based on their changes in the enthalpy of the reactions.

Experimentally, it was found that the two possible competitive QMT reactions are affected differently by the nature of the C4 electron-donating substituents (Table 1):

(i) The rate of the QMT ring-opening **3** → ^{1}**2** exhibits greater variability, with half-lives ranging from 48 min to undetectable within the timescale of days. Moreover, the QMT reaction **3** → ^{1}**2** becomes faster as the electron-donating strength of the C4 substituent increases, i.e., $k_{\mathbf{2b}}$ and $k_{\mathbf{2d}} < k_{\mathbf{2c}} < k_{\mathbf{2e}} < k_{\mathbf{2f}}$. These observations align reasonably well with the computed QMT rates and can also be rationalized by the PES analysis, which demonstrates a correlation trend between the increase of the electron-donating strength of the C4 substituent and the decrease in the enthalpy of reaction (in conjugation with the decrease in the barrier height).

(ii) The rate of the QMT ring-expansion **3** → **4** exhibits smaller variability, with half-lives ranging from 1.9 to 12.8 h. Electron-donating substituents at C4 are important to decrease the rate of the QMT ring-expansion compared to the expected rate of the unsubstituted benzazirine, making the reactions amenable to experimental observation. However, a trend was not found between the set of electron-donating substituents and their QMT reaction rates for the **3** → **4** reaction (Table 1). These observations are fairly well reproduced by the computed QMT rates and are also compatible with the PES analysis, which suggests that the electron-donating C4 substituents induce at most a small increase in the enthalpy of the reaction (in conjugation with an increase in the barrier height), but without correlating with their respective strengths.

Remarkably, such a distinct substituent effect on the two QMT reactions enables us to attain control over the selectivity of the benzazirine QMT reactivity. We demonstrate here how to make the QMT ring-opening **3** → ^{1}**2** competitive with the QMT ring-expansion **3** → **4** as the electron-donating strength of the C4 substituent increases, up to a point where it becomes the dominant process for the strongest electron-donating substituent **2f** (Figure 7).

Table 1. Experimental QMT rates (k_{exp} in s^{-1}) and half-lives ($\tau_{1/2}$ in h) measured in Ar matrices at 3.5 K and computed QMT rates (k_{comp} in s^{-1}) for C4-substituted 2*H*-benzazirines **2**.[a]

C4 substituent	QMT ring-opening	k_{exp}	$\tau_{1/2}$	k_{comp}	QMT ring-expansion	k_{exp}	$\tau_{1/2}$	k_{comp}
H	**3a** → ^{1}**2a**	n.o.	n.o.	1.5×10^{-18}	**3a** → **4a**	n.o.	n.o.	7.5×10^{1}
SCH_3	**3b** → ^{1}**2b**	n.o.	n.o.	n.c.	**3b** → **4b**	1.5×10^{-5}	12.8	n.c.
OH	**3d** → ^{1}**2d**	n.o.	n.o.	2.8×10^{-11}	**3d** → **4d**	3.3×10^{-5}	5.8	2.0×10^{-4}
NH_2	**3c** → ^{1}**3c**	8.3×10^{-6}	23.3	1.9×10^{-3}	**4c** → **3c**	4.7×10^{-5}	4.1	3.3×10^{-4}
$N(CH_3)_2$	**3e** → ^{1}**2e**	1.1×10^{-5}	17.2	n.c.	**3e** → **4e**	2.6×10^{-5}	7.4	n.c.
$N(CH_2)_4$	**3f** → ^{1}**2f**	2.4×10^{-4}	0.8	1.3×10^{3}	**3e** → **4f**	1.0×10^{-4}	1.9	1.6×10^{-5}

[a]The QMT rates measured for **3b** and **3c** were published elsewhere (gray background).[24,27] The computed QMT rates of unsubstituted 2*H*-benzazirine **3a** (section 3 of the SI) is given for comparative purposes. Abbreviation n.o. stands for not observed whereas n.c. for not computed. In the case of thiomethyl **3b** and dimethylamino **3e** derivatives, the rotamerization of this group occurs concomitantly with the ring-opening or ring-expansion reaction, which makes it difficult to compute the corresponding PES accurately and limit our ability to provide meaningful QMT rates.

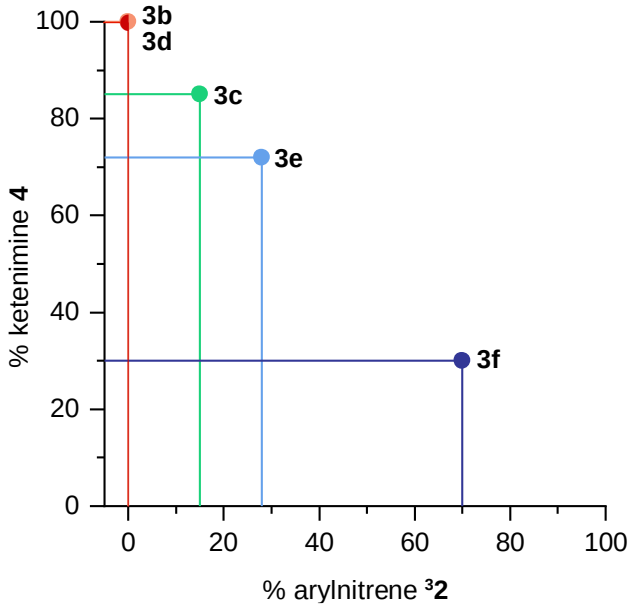

Figure 7. Product distribution of arylnitrene ^{3}**2** : ketenimine **4** (in %) formed by competitive QMT ring-opening *vs* ring-expansion reactions of benzazirine derivatives **3** in Ar matrices at 3 K in the dark. The product distribution of the QMT reactions of **3b** and **3c** were published elsewhere.[24,27]

3. CONCLUSIONS

We have investigated how QMT selectivity can be controlled by electronic substituent effects. Benzazirines **3** were used as model compounds due to their exceptional ability to react by two competitive QMT pathways. Three novel benzazirine targets with increasingly stronger electron-donating substituents at C4 [R = OH, $N(CH_3)_2$, and $N(CH_2)_4$] were successfully generated in argon matrices at 3−18 K, using the corresponding arylazides as starting precursors. Remarkably, QMT reactivity with different selectivity was observed for all three benzazirines. As the substituent electron-donating strength increases, the QMT ring-opening to nitrene **2** starts to compete with the QMT ring-expansion to ketenimine **4**, eventually dominating the process for the substituent with the highest electron-donating strength [$N(CH_2)_4$]. Computed QMT rates using the WKB model show qualitative agreement with the observed selectivity. The QMT ring-opening reaction **3** → **2** was found to be intrinsically more susceptible to substituent electronic effects than the QMT ring-expansion reaction **3** → **4**. An interesting correlation was shown between the increase in substituent electron-donating strength, the increase in the QMT ring-opening rate **3** → **2**, and the decrease in the corresponding enthalpy of reaction or barrier width (in conjugation with the decrease in the barrier height). Overall, this work reveals how subtle changes in electronic effects can be used to tune the QMT selectivity, and how the barrier widths, more than the barrier heights, are the determining factor. As harnessing QMT reactivity emerges as a promising approach to molecular design,[41,42] developing strategies to control QMT is essential. Our investigations provide fundamental insights into this fascinating field, which we hope will drive further advancements.

ASSOCIATED CONTENT

The supporting information (SI) includes: experimental and computational methods, additional experimental and theoretical results, vibrational assignments, and computational data.

AUTHOR INFORMATION

Corresponding Author

*cmnunes@qui.uc.pt

*prs@uni-giessen.de

Conflict of Interest

The authors declare no competing interests.

ACKNOWLEDGEMENTS

This work was supported by Project PTDC/QUI-QFI/1880/2020, funded by National Funds via the Portuguese Foundation for Science and Technology (FCT). The Coimbra Chemistry Centre – Institute of Molecular Sciences (CQC-IMS) is supported by FCT through projects UIDB/00313/2020 and UIDP/00313/2020 co-funded by COMPETE and the IMS special complementary funds provided by FCT. C.M.N. acknowledges FCT for an Auxiliary Researcher grant. J.P.L.R. acknowledges FCT for a PhD grant (https://doi.org/10.54499/2020.04467.BD). The authors acknowledge FCT Advanced Computing Project 2023.10449.CPCA and the Laboratory for Advanced Computing at University of Coimbra (UC-LCA) for providing computing resources that have contributed to the research results reported within this paper and Coimbra Laser Lab (CLL) for experimental facilities. This project has received funding from the European Research Council (ERC) under the European Union's Horizon 2020 research and innovation programme (Advanced Grant No. 101054751 "COLDOC" to P.R.S.). Views and opinions expressed are those of the authors only and do not necessarily reflect those of the European Union or the European Research Council.

REFERENCES

(1) Eyring, H. The Activated Complex in Chemical Reactions. *J. Chem. Phys.* **1935**, *3*, 63–71.

(2) Evans, M. G.; Polanyi, M. Some Applications of the Transition State Method to the Calculation of Reaction Velocities, Especially in Solution. *Trans. Faraday Soc.* **1935**, *31*, 875–894.

(3) M. G. Evans; M. Polanyi. Further Considerations on the Thermodynamics of Chemical Equilibria And Reaction Rates. *Trans. Faraday Soc.* **1936**, *32*, 1333–1360.

(4) Bell, R. P. The Theory of Reactions Involving Proton Transfers. *Proc. R. Soc. London. A* **1936**, *154*, 414–429.

(5) Hammond, G. S. A Correlation of Reaction Rates. *J. Am. Chem. Soc.* **1955**, *77*, 334–338.

(6) Schreiner, P. R.; Reisenauer, H. P.; Ley, D.; Gerbig, D.; Wu, C. H.; Allen, W. D. Methylhydroxycarbene: Tunneling Control of a Chemical Reaction. *Science* **2011**, *332*, 1300–1303.

(7) Schreiner, P. R. Tunneling Control of Chemical Reactions: The Third Reactivity Paradigm. *J. Am. Chem. Soc.* **2017**, *139*, 15276–15283.

(8) Knapp, M. J.; Rickert, K.; Klinman, J. P. Temperature-Dependent Isotope Effects in Soybean Lipoxygenase-1: Correlating Hydrogen Tunneling with Protein Dynamics. *J. Am. Chem. Soc.* **2002**, *124*, 3865–3874.

(9) Roque, J. P. L.; Nunes, C. M.; Viegas, L. P.; Pereira, N. A. M.; Pinho e Melo, T. M. V. D.; Schreiner, P. R.; Fausto, R. Switching on H-Tunneling through Conformational Control. *J. Am. Chem. Soc.* **2021**, *143*, 8266–8271.

(10) Kirshenboim, O.; Frenklah, A.; Kozuch, S. Switch Chemistry at Cryogenic Conditions: Quantum Tunnelling under Electric Fields. *Chem. Sci.* **2021**, *12*, 3179–3187.

(11) Schleif, T.; Prado Merini, M.; Henkel, S.; Sander, W. Solvation Effects on Quantum Tunneling Reactions. *Acc. Chem. Res.* **2022**, *55*, 2180–2190.

(12) Nandi, A.; Gerbig, D.; Schreiner, P. R.; Borden, W. T.; Kozuch, S. Isotope-Controlled Selectivity by Quantum Tunneling: Hydrogen Migration versus Ring Expansion in Cyclopropylmethylcarbenes. *J. Am. Chem. Soc.* **2017**, *139*, 9097–9099.

(13) Galabov, B.; Ilieva, S.; Cheshmedzhieva, D.; Nikolova, V.; Popov, V. A.; Hadjieva, B.; Schaefer, H. F. Mini-Review on Structure-Reactivity Relationship for Aromatic Molecules: Recent Advances. *ACS Omega* **2022**, *7*, 8199–8208.

(14) Carey, F. A.; Sundberg, R. J. *Advanced Organic Chemistry Part A: Structure and Mechanisms*, 5th ed.; Springer: New York, 2007; pp 335–344.

(15) Qiu, G.; Schreiner, P. R. The Intrinsic Barrier Width and Its Role in Chemical Reactivity. *ACS Cent. Sci.* **2023**, *9*, 2129–2137.

(16) Schleif, T.; Tatchen, J.; Rowen, J. F.; Beyer, F.; Sanchez-Garcia, E.; Sander, W. Heavy-Atom Tunneling in Semibullvalenes: How Driving Force, Substituents, and Environment Influence the Tunneling Rates. *Chem. Eur. J.* **2020**, *26*, 10452–10458.

(17) Amiri, S.; Reisenauer, H. P.; Schreiner, P. R. Electronic Effects on Atom Tunneling: Conformational Isomerization of Monomeric Para-Substituted Benzoic Acid Derivatives. *J. Am. Chem. Soc.* **2010**, *132*, 15902–15904.

(18) Meisner, J.; Kästner, J. Atom Tunneling in Chemistry. *Angew. Chem. Int. Ed.* **2016**, *55*, 5400–5413.

(19) Layfield, J. P.; Hammes-Schiffer, S. Hydrogen Tunneling in Enzymes and Biomimetic Models. *Chem. Rev.* **2014**, *114*, 3466–3494.

(20) Buchwalter, S. L.; Gloss, G. L. An Electron Spin Resonance Study of Matrix Isolated 1,3-Cyclopentadiyl, a Localized 1,3-Carbon Biradical. *J. Am. Chem. Soc.* **1975**, *97*, 3857–3858.

(21) Castro, C.; Karney, W. L. Heavy-Atom Tunneling in Organic Reactions. *Angew. Chem. Int. Ed.* **2020**, *59*, 8355–8366.

(22) Nunes, C. M.; Reva, I.; Fausto, R. Direct Observation of Tunnelling Reactions by Matrix Isolation Spectroscopy. In *Tunnelling in Molecules: Nuclear Quantum Effects from Bio to Physical Chemistry*; Kästner, J., Kozuch, S., Eds. The Royal Society of Chemistry, 2021; pp 1–60.

(23) Fausto, R.; Ildiz, G. O.; Nunes, C. M. IR-Induced and Tunneling Reactions in Cryogenic Matrices: The (Incomplete) Story of a Successful Endeavor. *Chem. Soc. Rev.* **2022**, *51*, 2853–2872.

(24) Inui, H.; Sawada, K.; Oishi, S.; Ushida, K.; McMahon, R. J. Aryl Nitrene Rearrangements: Spectroscopic Observation of a Benzazirine and Its Ring Expansion to a Ketenimine by Heavy-Atom Tunneling. *J. Am. Chem. Soc.* **2013**, *135*, 10246–10249.

(25) Schleif, T.; Mieres-Perez, J.; Henkel, S.; Mendez-Vega, E.; Inui, H.; McMahon, R. J.; Sander, W. Conformer-Specific Heavy-Atom Tunneling in the Rearrangement of Benzazirines to Ketenimines. *J. Org. Chem.* **2019**, *84*, 16013–16018.

(26) Nunes, C. M.; Reva, I.; Kozuch, S.; McMahon, R. J.; Fausto, R. Photochemistry of 2-Formylphenylnitrene: A Doorway to Heavy-Atom Tunneling of a Benzazirine to a Cyclic Ketenimine. *J. Am. Chem. Soc.* **2017**, *139*, 17649–17659.

(27) Nunes, C. M.; Eckhardt, A. K.; Reva, I.; Fausto, R.; Schreiner, P. R. Competitive Nitrogen versus Carbon Tunneling. *J. Am. Chem. Soc.* **2019**, *141*, 14340–14348.

(28) Nunes, C. M.; Doddipatla, S.; Loureiro, G. F.; Roque, J. P. L.; Pereira, N. A. M.; Pinho e Melo, T. M. V. D.; Fausto, R. Differential Tunneling-Driven and Vibrationally-Induced Reactivity in Isomeric Benzazirines. *Chem. Eur. J.* **2022**, *28*, e202202306.

(29) Kozuch, S. On the Tunneling Instability of a Hypercoordinated Carbocation. *Phys. Chem. Chem. Phys.* **2015**, *17*, 16688–16691.

(30) Amlani, H.; Frenklah, A.; Kozuch, S. Tunnelling Instability in Molecular Systems. An Exercise in Computational Chemistry Prediction Power. In *Tunnelling in Molecules: Nuclear Quantum Effects from Bio to Physical Chemistry*; Kästner, J., Kozuch, S., Eds. The Royal Society of Chemistry, 2021; pp 61–87.

(31) Hayes, J. C.; Sheridan, R. S. Infrared Spectrum of Triplet Phenylnitrene. On the Origin of Didehydroazepine in Low-Temperature Matrices. *J. Am. Chem. Soc.* **1990**, *112*, 5879–5881.

(32) Mieres-Pérez, J.; Mendez-Vega, E.; Velappan, K.; Sander, W. Reaction of Triplet Phenylnitrene with Molecular Oxygen. *J. Org. Chem.* **2015**, *80*, 11926–11931.

(33) Karney, W. L.; Borden, W. T. Ab Initio Study of the Ring Expansion of Phenylnitrene and Comparison with the Ring Expansion of Phenylcarbene. *J. Am. Chem. Soc.* **1997**, *119*, 1378–1387.

(34) Johnson, W. T. G.; Sullivan, M. B.; Cramer, C. J. Meta and Para Substitution Effects on the Electronic State Energies and Ring-Expansion Reactivities of Phenylnitrenes. *Int. J. Quantum Chem.* **2001**, *85*, 492–508.

(35) Hansch, C.; Leo, A.; Taft, R. W. A Survey of Hammett Substituent Constants and Resonance and Field Parameters. *Chem. Rev.* **1991**, *91*, 165–195.

(36) In **1d** the hydroxyl group can adopt *syn*- and *anti*-conformation relative to the azide group. However, it is known that fast OH-rotamerization occurs from the high-energy to the low-energy conformation of phenol derivatives in an argon matrix. Therefore, only the most stable phenol derivative conformer can be detected under these conditions. Hence, here we assume only the existence of the most stable hydroxyl group conformation for the arylazide

1d and its photoproducts. A detailed discussion of this topic is addressed elsewhere.[28] For a theoretical discussion on a molecular quantum switch based on OH-rotamerization tunneling of a phenol derivative, see: (a) Fabri. C.; Albert, S.; Chen, Z.; Prentner, R.; Quack, M. *Phys. Chem. Chem. Phys.* **2018**, *20*, 7387–7394.

(37) Quanz, H.; Schreiner, P. R. TUNNEX: An Easy-to-Use Wentzel-Kramers-Brillouin (WKB) Implementation to Compute Tunneling Half-Lives. *J. Comput. Chem.* **2019**, *40*, 543–547.

(38) The width of a potential energy barrier relevant for QMT was obtained as the distance between the two classical turning points (see more details in section 2.3 and Table S13 of the SI). Those are defined as the points where the total energy of the system is equal to the potential, i.e., the points where the energy at the vibrational ground state of the reactant intersects the potential energy surface.

(39) Structure **3f'** is a minimum at the B3LYP/6-311+G(2d,p) level but has a small imaginary frequency (34*i* cm^{-1}) at the CASSCF(8,8)/6-311+G(2d,p) level. Therefore, the IRC describing the **3f'** → **^{1}2f'** reaction computed at the CASSCF(8,8) had to be truncated at a geometry similar to **3f'**. Thus, the **3f'** → **^{1}2f'** QMT reaction rate is a rough estimation.

(40) QMT reactivity also depends on the shape of the PES of a reaction. Actually, the one-dimensional barrier width may not be a completely reliable indicator for QMT reactivity. These two points are well illustrated in section 4 of the SI. A more precise indicator for QMT reactivity might be the area of the permeation barrier.

(41) Constantin, T.; Górski, B.; Tilby, M. J.; Chelli, S.; Juliá, F.; Llaveria, J.; Gillen, K. J.; Zipse, H.; Lakhdar, S.; Leonori, D. Halogen-Atom and Group Transfer Reactivity Enabled by Hydrogen Tunneling. *Science* **2022**, *377*, 1323–1328.

(42) Bae, S. H.; Li, X.-X.; Seo, M. S.; Lee, Y.-M.; Fukuzumi, S.; Nam, W. Tunneling Controls the Reaction Pathway in the Deformylation of Aldehydes by a Nonheme Iron(III)-Hydroperoxo Complex: Hydrogen Atom Abstraction versus Nucleophilic Addition. *J. Am. Chem. Soc.* **2019**, *141*, 7675–7679.